Direct Kinetics Study of the Temperature Dependence of the CH_2O Branching Channel for the CH_3O_2 + HO_2 Reaction

MATTHEW J. ELROD, DANA L. RANSCHAERT, NICHOLAS J. SCHNEIDER

Department of Chemistry, Hope College, Holland, Michigan, 49423

Received 8 September 2000; accepted 26 January 2001

ABSTRACT: A direct kinetics study of the temperature dependence of the CH_2O branching channel for the CH_3O_2 + HO_2 reaction has been performed using the turbulent flow technique with high-pressure chemical ionization mass spectrometry for the detection of reactants and products. The temperature dependence of the CH_2O-producing channel rate constant was investigated between 298 and 218 K at a pressure of 100 Torr, and the data were fitted to the following Arrhenius expression: $1.6^{+1.0}_{-0.7} \times 10^{-15} \times \exp[(1730 \pm 130)/T]$ cm^3 molecule^{-1} s^{-1}. Using the Arrhenius expression for the overall rate of the CH_3O_2 + HO_2 reaction and this result, the 298 K branching ratio for the CH_2O producing channel is measured to be 0.11, and the branching ratio is calculated to increase to a value of 0.31 at 218 K, the lowest temperature accessed in this study. The results are compared to the analogous CH_3O_2 + CH_3O_2 reaction and the potential atmospheric ramifications of significant CH_2O production from the CH_3O_2 + HO_2 reaction are discussed. © 2001 John Wiley & Sons, Inc. Int J Chem Kinet 33: 363–376, 2001

INTRODUCTION

The methylperoxy radical (CH_3O_2) is an important intermediate species formed in the oxidation of methane in the atmosphere [1].

$$CH_4 + OH \longrightarrow CH_3 + H_2O \quad (1)$$

$$CH_4 + O(^1D) \longrightarrow CH_3 + OH \quad (2)$$

$$CH_3 + O_2 + M \longrightarrow CH_3O_2 + M \quad (3)$$

Ozone levels in the atmosphere are directly affected by CH_3O_2 reactions, which themselves are dependent on the levels of the nitrogen oxides (NO_x). Under high NO_x conditions (generally, lower tropospheric conditions), CH_3O_2 reactions lead to the production of ozone, the most deleterious constituent of photochemical smog.

$$CH_3O_2 + NO \longrightarrow CH_3O + NO_2 \quad (4a)$$

$$NO_2 + h\nu\,(\lambda < 380\text{ nm}) \longrightarrow NO + O \quad (5)$$

$$O + O_2 + M \longrightarrow O_3 + M \quad (6)$$

CH_3O_2 can also be temporarily removed from the ozone production cycles by the formation of reservoir species.

$$CH_3O_2 + NO + M \longrightarrow CH_3ONO_2 + M \quad (4b)$$

Correspondence to: M. J. Elrod (elrod@hope.edu)

$$CH_3O_2 + HO_2 \longrightarrow CH_3OOH + O_2 \quad (7a)$$

$$\longrightarrow CH_2O + H_2O + O_2 \quad (7b)$$

A potential product of reaction 4, CH_3ONO_2 (from reaction 4b), has been directly measured in the atmosphere and suggested as a tracer of the photochemical age of air masses [2], but the chemical processes leading to its presence in the atmosphere remain unclear [3], despite recent attempts to establish the atmospheric significance of reaction 4b [4]. Recently, Wennberg et al. [5] reported the measurement of higher HO_x levels than predicted in the upper troposphere of the northern hemisphere, suggesting that this region of the atmosphere is more susceptible to NO_x-catalyzed ozone production than previously thought. This is an important result since it significantly impacts models that predict the effect of aviation on ozone levels in the atmosphere. Therefore, it is critical to obtain the relative rates of reaction 4 and reaction 7 and to understand the product distributions of these reactions in order to address the impact of CH_3O_2 chemistry on this issue.

In the first phase of addressing these issues for CH_3O_2 chemistry, we investigated reaction 4 by measuring the temperature dependence of the overall rate constant for the CH_3O_2 + NO reaction and establishing an upper limit for the CH_3ONO_2-producing branching channel [4]. This article details the second phase of this work: an investigation of the kinetics of the CH_3O_2 + HO_2 reaction. The overall rate constant k_7 for this reaction has received considerable previous study by flash photolysis (FP) techniques [6–13]. As the JPL recommendation for the overall rate constant for this reaction states [14], the agreement among the various studies is not very good. The lack of a consensus result for this rate constant is most likely due to the near universal use of overlapping HO_2 and CH_3O_2 UV absorption detection methods (for which different UV cross sections have been used in the determination of the absolute rate constants) and the complicated secondary chemistry resulting from the peroxy radical self-reactions (CH_3O_2 + CH_3O_2 and HO_2 + HO_2).

As for the CH_3O_2 + NO reaction, a secondary branching channel for the CH_3O_2 + HO_2 reaction has also been proposed:

$$CH_3O_2 + HO_2 \longrightarrow CH_2O + H_2O + O_2 \quad (7b)$$

There have been several investigations of the CH_3OOH-producing rate constant k_{7a} [9,15,16] as well as one indirect investigation of the CH_2O-producing rate constant k_{7b} (using the isotopically substituted CD_3O_2 reactant and detecting the HDO product from reaction 7b) [8]. These studies are in fairly wide disagreement, with estimates for the secondary CH_2O-producing channel branching ratio [$k_{7b}/(k_{7a} + k_{7b})$] ranging from as low as zero [16] to as high as 0.40 [8]. Indeed, because of this lack of agreement, the JPL recommendation for the CH_3O_2 + HO_2 reaction specifically calls for new studies using direct CH_2O detection techniques [14]. Because the products CH_3OOH (from reaction 7a) and CH_2O (from reaction 7b) are characterized by quite different photochemical reactivity (with a potentially varying impact on HO_x cycling and O_3 production efficiency), it is very important to quantitatively establish the atmospheric relevance of reaction 7b. In addition, it has been suggested by Ayers et al. [17] and Weller et al. [18] that the underprediction by atmospheric models (which generally assumes a zero branching ratio value for reaction (7b)) of CH_2O levels in the remote troposphere may be a consequence of a significant CH_2O-forming product channel for the CH_3O_2 + HO_2 reaction.

In this article we describe our investigation of the kinetics of the CH_3O_2 + HO_2 reaction conducted at pressures near 100 Torr and at a range of temperatures extending to those found in the upper troposphere using a turbulent flow (TF) tube coupled to a high-pressure chemical ionization mass spectrometer (CIMS). It has been previously shown that TF technique can be used to accurately determine the rate constants of reactions at pressures ranging from 50 to 760 Torr and at temperatures as low as 180 K [19]. As in our previous kinetics studies of the CH_3O_2 + NO and $C_2H_5O_2$ + NO reactions using the coupled TF-CIMS approach [4,20], we are able to directly access atmospheric pressure and temperature conditions and sensitively monitor many of the relevant reactants and products for the CH_3O_2 + HO_2 reaction. In contrast to previous work on this reaction, we are able to unambiguously monitor both reactants (CH_3O_2 and HO_2) as well as a species (CH_3OOH or CH_2O) from each of the potential product channels 7a and 7b. This capability allows for the first direct product study of reaction 7b.

EXPERIMENTAL

Turbulent Fast-Flow Tube Kinetics

A schematic of the experimental apparatus is presented in Figure 1 and is similar to that used in a previous study of HO_2 + BrO [21] with the BrO source

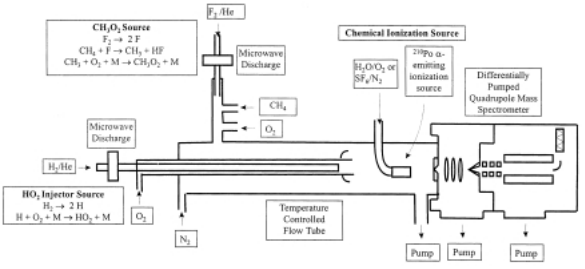

Figure 1 Experimental apparatus.

replaced by the CH_3O_2 source described in Scholtens et al. [4] The flow tube was constructed with 2.2 cm i.d. Pyrex tubing and was 60 cm in total length. A large flow of nitrogen carrier gas (approximately 30 STP liter min^{-1}) was injected at the rear of the flow tube. The gases necessary to generate CH_3O_2 were introduced through a 10-cm-long, 12.5-mm diameter sidearm located at the rear of the flow tube. HO_2 was generated in a triple-nested movable injector. The outer encasement (made from corrugated Teflon tubing) was used so that the injector could be moved to various injector positions without breaking any vacuum seals, as well as to prevent ambient gases from condensing on cold portions of the injector. A fan-shaped Teflon device was placed at the end of the injector in order to enhance turbulent mixing. The polonium-210, alpha-emitting ionization source was placed between the temperature-regulated flow tube and the inlet to the quadrupole mass spectrometer. Most of the flow-tube gases were removed at the CIMS inlet by a 31-L s^{-1} roughing pump. All gas flows were monitored with calibrated mass flow meters. The flow-tube pressure was measured upstream of the ionization source using a 0–1,000 Torr capacitance manometer. The temperature was determined at both the entrance and exit points of the temperature-regulated region of the flow tube using Cu–constantan thermocouples.

Reactant Preparation

CH_3O_2 was generated using the following reactions:

$$CH_4 + F \longrightarrow CH_3 + HF \qquad (8)$$

$$CH_3 + O_2 + M \longrightarrow CH_3O_2 + M \qquad (9)$$

($k_8 = 6.7 \times 10^{-11}$ cm^3 $molecule^{-1}$ s^{-1} and $k_9 = 4.9 \times 10^{-13}$ cm^3 $molecule^{-1}$ s^{-1} at 100 Torr) [14]. Fluorine atoms were produced by combining a 2.0 STP liter min^{-1} flow of helium (99.999%), which had passed through a silica gel trap immersed in liquid nitrogen, with a 0.5–5.0 STP ml min^{-1} flow of a 1% F_2/He mixture (Excimer grade), which then passed through a microwave discharge produced by a Beenakker cavity operating at 50 W. To generate CH_3, the fluorine atoms were then injected into a sidearm and mixed with an excess of CH_4 (CP grade, $\sim 10^{15}$ molecule cm^{-3}) in order to ensure that no fluorine atoms were introduced into the main flow. CH_3O_2 was then produced by the addition of an excess of O_2 (99.995%; $\sim 1 \times 10^{16}$ molecule cm^{-3}) just downstream of the production of CH_3. Absolute CH_3O_2 concentrations were determined by the titration reaction:

$$CH_3O_2 + NO \longrightarrow CH_3O + NO_2 \qquad (10)$$

($k_{10} = 7.8 \times 10^{-12}$ cm^3 $molecule^{-1}$ s^{-1}) [14] and subsequent calibration of the NO_2 mass spectrometer signal. Computer modeling of these titration conditions indicates that slightly more NO_2 is produced than CH_3O_2 initially present because of the following secondary reactions:

$$CH_3O + O_2 \longrightarrow CH_2O + HO_2 \qquad (11)$$

$$HO_2 + NO \longrightarrow OH + NO_2 \qquad (12)$$

($k_{11} = 1.9 \times 10^{-15}$ cm^3 $molecule^{-1}$ s^{-1} and $k_{12} = 8.2 \times 10^{-12}$ cm^3 $molecule^{-1}$ s^{-1}) [14]. Therefore, the measured NO_2 concentrations must be adjusted to determine the correct $[CH_3O_2]_0$ value. However, for typical O_2 and NO concentrations, the conversion factor was close to unity ($[NO_2]_{titration} = 1.08\ [CH_3O_2]_0$) because the following reaction was dominant over reaction (11):

$$CH_3O + NO + M \longrightarrow CH_3ONO + M \qquad (13)$$

($k_{13} = 1.3 \times 10^{-11}$ cm^3 $molecule^{-1}$ s^{-1} at 100 Torr) [14]. Reaction 13 has a smaller branching channel to produce HNO and CH_2O, but since neither of these products produces or consumes NO_2 under our flow reactor conditions, it is not expected to impact the titration results. NO_2 impurities in the NO (CP grade) used in reaction (10) were removed by the use of a dry ice/methanol-cooled silica gel trap placed between the NO reservoir (usually a 3% mixture in N_2) and the flow tube. For this study, CH_3O_2 concentrations ranged from about 3 to 10×10^{11} molecule cm^{-3}.

HO_2 was generated from the following reaction:

$$H + O_2 + M \longrightarrow HO_2 + M \qquad (14)$$

($k_{14} = 2.0 \times 10^{-13}$ cm^3 $molecule^{-1}$ s^{-1} at 100 Torr)

[14]. Because HO_2 was introduced through a movable injector where the corresponding concentrations are ~30 times higher than in the main flow tube, the disproportionation reaction:

$$HO_2 + HO_2 (+M) \longrightarrow H_2O_2 + O_2 (+M) \quad (15)$$

($k_{15} = 1.8 \times 10^{-12}$ cm^3 molecule^{-1} s^{-1} at 100 Torr) [14] is a concern in the production of large quantities of HO_2. By taking advantage of the long lifetime of H-atoms, this difficulty was surmounted by using a nested injector that kept the hydrogen atoms (entrained in the inner 3-mm alumina tube) and oxygen molecules (entrained in the outer 6-mm Pyrex tube) separate throughout all but the last 1 cm of the injector. The hydrogen atoms were allowed to mix with a very large excess of O_2 (~3×10^{17} molecule cm^{-3} inside the injector) for only about 1 ms, allowing reaction 14 to virtually go to completion, but preventing significant self-reaction of HO_2. Hydrogen atoms were generated by combining a 5.0 STP L min^{-1} flow of helium (99.999%, which had passed through a liquid-nitrogen-cooled silica gel trap) with a 0.5 to 4.0 STP mL min^{-1} flow of a 10% H_2(99.9%)/He mixture, which was then sent through a microwave discharge produced by a Beenaker cavity operating at 70 W. Absolute HO_2 concentrations were determined in a fashion similar to that for CH_3O_2:

$$HO_2 + NO \longrightarrow OH + NO_2 \quad (12)$$

followed by calibration of the NO_2 mass spectrometer signal.

CH_2O Branching-Channel Measurements

In these studies, the production of CH_2O from reaction (7b) was monitored directly over a reaction time of ~25 ms. The absolute reaction times were calculated from the flow velocity and the distance between the injector and the mass spectrometer sampling aperture. Computer modeling was used to extract the rate constant k_{7b} from the observed production of CH_2O and the initial concentrations of all relevant chemical species. In order to determine the detection sensitivity of the mass spectrometer for CH_2O, two different calibration methods were employed. The first method involved the preparation of a standard sample of CH_2O and the introduction of a metered flow of CH_2O to the system. The standard CH_2O sample was prepared by heating paraformaldehyde and transferring the vapor to a carefully dried glass bulb. The CH_2O was then diluted with N_2 and added to the system for direct mass-spectrometric calibration. This procedure was somewhat troublesome in that the mass-spectrometer signal depended on the time elapsed since the sample was prepared. This effect was probably due to a drop in the gaseous CH_2O concentration as a result of the reformation of paraformaldehyde on the glass bulb walls or on the surfaces of the mass flow meter. Although a regular remixing of the CH_2O standard sample solved this problem, we choose to employ a more convenient, alternative CH_2O calibration method. This second method takes advantage of the chemistry of the CH_3O_2/NO calibration:

$$CH_3O_2 + NO \longrightarrow CH_3O + NO_2 \quad (10)$$

$$CH_3O + O_2 \longrightarrow CH_2O + HO_2 \quad (11)$$

By using high O_2 concentrations, most of the CH_3O_2 reactant can be converted to CH_2O, with the result that a secondary calibration for CH_2O can be made by reference to the NO_2 calibration that is part of the CH_3O_2 procedure. In order to effect the most advantageous conditions, we used O_2 as the carrier gas for the CH_3O_2/NO titration/calibration experiments (for experiments at 100 Torr total pressure, $[O_2] > 3.0 \times 10^{18}$ molecule cm^{-3}), so that nearly all of the CH_3O_2 initially present is converted to CH_2O (for typical conditions, $[CH_2O] = 0.8[CH_3O_2]$) . Since the CH_2O for this calibration process is generated *in situ*, the problems with paraformaldehyde formation are avoided. Therefore, the CH_3O_2/NO titration/calibration approach was routinely used for CH_2O calibration, while the direct standard sample CH_2O method was used only occasionally to ensure the consistency of the two approaches.

Chemical Ionization Mass Spectrometric Detection

A positive ion chemical ionization scheme (with $H_3O^+(H_2O)_3$ as the reagent ion) was used to detect CH_3O_2, CH_3OOH, and CH_2O and a negative ion chemical ionization scheme (with SF_6^- as the reagent ion) was used to detect HO_2 and NO_2 with the quadrupole mass spectrometer. H_3O^+ was produced in the ion source by passing a large O_2 flow (5 STP L min^{-1}) through the polonium-210 alpha-emitting ionization source (with H_2O impurities being sufficiently abundant to produce sufficient quantities of reagent ions). SF_6^- was produced in the ion source by passing a large N_2 flow (5 STP L min^{-1}) and 1.0 STP mL min^{-1} of a 10 % SF_6/N_2 mixture through the ionization source. The commercial ionization source consisted of a hol-

low cylindrical (length: 69 mm; diameter: 12.7 mm) aluminum body with 10 mCurie (3.7×10^8 disintegrations s^{-1}) of polonium-210 coated on the interior walls.

Ions were detected with a quadrupole mass spectrometer housed in a two-stage differentially pumped vacuum chamber. Flow tube gases (neutrals and ions) were drawn into the front chamber through a 0.1-mm aperture, which was held at a potential of ±210 V. The ions were focused by three lenses constructed from 3.8-cm i.d., 4.8-cm o.d. aluminum gaskets. The front chamber was pumped by a 6-inch, 2,400 L s^{-1} diffusion pump. The gases entered the rear chamber through a skimmer cone with a 1.0-mm orifice (held at ±130 V), which was placed approximately 5 cm from the front aperture. The rear chamber was pumped by a 250-L s^{-1} turbomolecular pump. Once the ions passed through the skimmer cone, they were mass filtered and detected with a quadrupole mass spectrometer.

Chemical Ionization Schemes

The following chemical ionization schemes were used to detect the species CH_3O_2, CH_3OOH, CH_2O, HO_2, and NO_2:

$$CH_3O_2 + H_3O^+(H_2O)_3 \longrightarrow CH_3OOH^+(H_2O)_3 + H_2O \quad (16)$$

$$CH_3OOH + H_3O^+(H_2O)_3 \longrightarrow CH_3OOH_2^+(H_2O)_3 + H_2O \quad (17)$$

$$CH_2O + H_3O^+(H_2O)_3 \longrightarrow CH_2OH^+(H_2O)_3 + H_2O \quad (18)$$

$$HO_2 + SF_6^- \longrightarrow SF_4O_2^- + \text{other products} \quad (19)$$

$$NO_2 + SF_6^- \longrightarrow NO_2^- + SF_6 \quad (20)$$

The rates of reactions (18) and (20) have been measured previously ($k_{18} = 1.4 \times 10^{-9}$ cm^3 $molecule^{-1}$ s^{-1} and $k_{20} = 1.4 \times 10^{-10}$ cm^3 $molecule^{-1}$ s^{-1}) [22,23], reaction (16) has been used in our previous study of the CH_3O_2 + NO reaction [4], reaction (19) has been used in a previous study of the HO_2 + BrO reaction [21], and reaction (17) had been predicted to be thermodynamically feasible on the basis of electronic structure calculations [24].

For the low-temperature studies, liquid-nitrogen-cooled silicone oil was used as the coolant for the jacketed flow tube, and the nitrogen carrier gas was precooled by passing it through a copper coil immersed in a liquid N_2 reservoir followed by resistive heating. The temperature was controlled in the reaction region to within 1 K.

RESULTS AND DISCUSSION

Overview of Measurements

The use of relatively low concentrations of reactants (to minimize peroxy–peroxy self-reaction), relatively large flow velocities (necessary to ensure turbulent flow conditions) and a relatively small overall rate constant prevented the carrying out of a pseudo-first-order kinetics study of the overall rate constant. Instead, reactants and products were monitored as a function of time, and kinetics models were used to compare and/or fit the desired rate constants. The relevant reactions for kinetic modeling of the system are given in Table I. In this study, absolute concentration calibrations were obtained for CH_3O_2 and CH_2O, thus allowing direct use of the kinetics data for these species. Because of the critical importance of the accuracy of the CH_2O calibration approach, a comparison of the two CH_2O calibration methods is presented in Figure 2, illustrating the consistency of the two techniques.

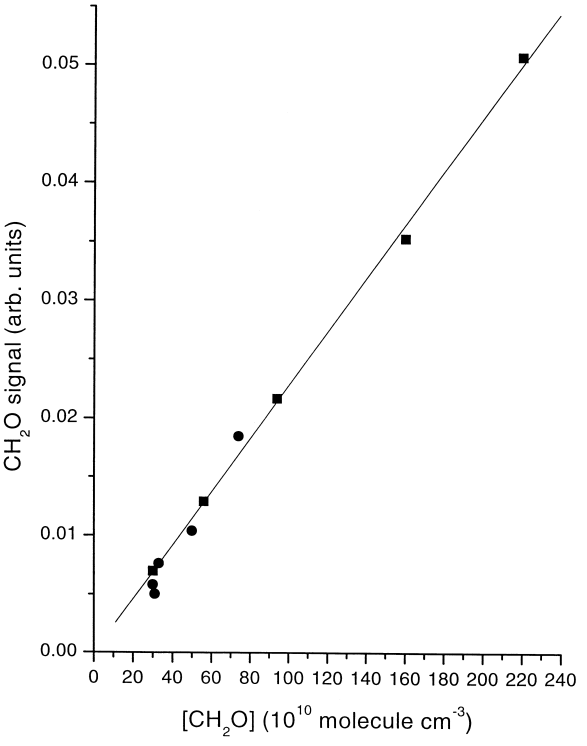

Figure 2 Comparison of CH_2O calibration methods (■: standard sample method; ●: CH_3O_2 + NO + O_2 titration method).

Table I Kinetics Parameters for Branching Ratio Determination

Reaction[a]	A ($cm^3\ s^{-1}$ $molecule^{-1}$)	E_a/R (K)
$CH_3O_2 + HO_2 \longrightarrow$ products	3.8×10^{-13}	−800
$CH_3O_2 + CH_3O_2 \longrightarrow CH_3OOCH_3 + O_2$	$2.5 \times 10^{-13} \times 0.1$	−190
$CH_3O_2 + CH_3O_2 \longrightarrow CH_3O + CH_3O + O_2$	$2.5 \times 10^{-13} \times$ f(T)[b]	−190
$CH_3O_2 + CH_3O_2 \longrightarrow CH_2O + CH_3OH + O_2$	$2.5 \times 10^{-13} \times (0.9 -$ f(T))	−190
$HO_2 + HO_2 \longrightarrow H_2O_2 + O_2$	2.3×10^{-13}	−600
$HO_2 + HO_2 + M \longrightarrow H_2O_2 + O_2 + M$	$1.7 \times 10^{-33} \times$ [M]	−1000
$CH_3O + O_2 \longrightarrow CH_2O + HO_2$	3.9×10^{-14}	900
$CH_3O + CH_3O_2 \longrightarrow CH_2O + CH_3OOH$[c]	2.6×10^{-12}	0
$CH_3O + CH_3O \longrightarrow CH_2O + CH_3OH$[d]	1.3×10^{-11}	0
$HO_2 + CH_2O \longrightarrow$ adduct	6.7×10^{-15}	−600

[a] Rate constants calculated from $k(T) = Ae^{-E_a/RT}$. All rate constant parameters from the JPL compilation (DeMore, W. B.; Sander, S. P.; Howard, C. J.; Ravishankara, A. R.; Golden, D. M.; Kolb, C. E.; Hampson, R. F.; Kurylo, M. J.; Molina, M. J. Chemical Kinetics and Photochemical Data for Use in Stratospheric Modeling, JPL Publication 97-4; Jet Propulsion Laboratory: Pasadena, California, 1997), unless otherwise indicated.

[b] Temperature-dependent branching ratio calculated from $f(T) = \left[1 + e^{\left(\frac{1131}{T} - 294\right)}\right]^{-1}$

[c] Rate constant parameters from Heicklen, J.; Adv Photochem 1988, 14, 177.

[d] Rate constant parameters from Biggs, P.; Canosa-Mas, C. E.; Fracheboud, J.-M.; Shallcross, D. E.; Wayne, R. P. J Chem Soc Faraday Trans. 1997, 93, 2481.

An approximate calibration for CH_3OOH (constructed by using the same mass spectrometer sensitivity factor as was determined for CH_3O_2) was used in order to allow an estimate of the rate of formation of this product. Typical concentration vs. time profiles for the species CH_3O_2 and CH_3OOH are presented in Figures 3 and 4, respectively. In order to facilitate discussion of background contributions to the observed CH_2O signal, the raw data (signal vs. injector distance) collected for the CH_2O profiles are presented in Figure 5, and the time-dependent production of CH_2O (with several different assumed values for k_{7b} overlaid) is presented in Figure 6. HO_2 profiles were not routinely collected because HO_2 concentrations were generally not significantly varied ($\sim 1.2 \times 10^{12}$ molecule cm^{-3}), and the decay profiles of HO_2 were significantly influenced by the $HO_2 + HO_2$ self-reaction.

Overall Rate-Constant Evaluation

Figure 3 contains a kinetics plot ($[CH_3O_2]$ vs. time) for an experiment performed at 100 Torr and 298 K (squares), as well as the predicted CH_3O_2 decay (solid line) from a model calculation using the calibrated initial concentrations of CH_3O_2 and HO_2 and the reactions listed in Table I. As the graph indicates, there is good agreement between our experimental data and modeling results that employ the JPL recommendation [14] for the overall rate constant for $CH_3O_2 + HO_2$ (which is based on the earlier FP studies). We also find that our temperature-dependence results for

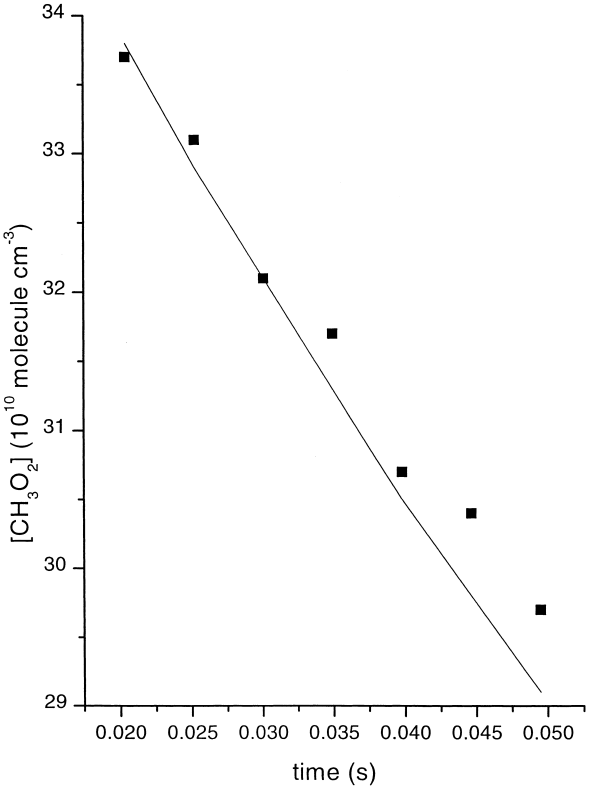

Figure 3 $[CH_3O_2]$ vs. time for the $CH_3O_2 + HO_2$ reaction at 100 Torr, 298 K, $[CH_3O_2]_0 = 3.8 \times 10^{11}$ molecule cm^{-3} and $[HO_2]_0 = 1.0 \times 10^{12}$ molecule cm^{-3} (■: actual data; ———: model).

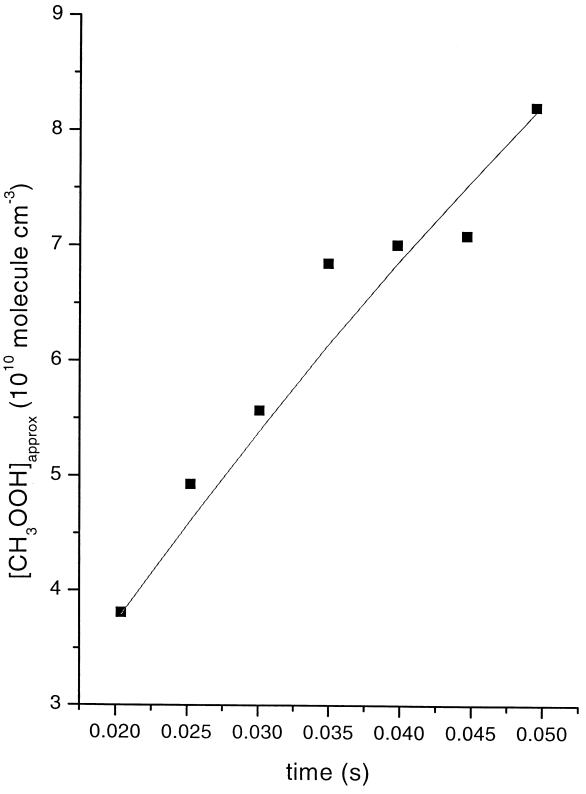

Figure 4 $[CH_3OOH]_{approx}$ vs. time for the CH_3O_2 + HO_2 reaction at 100 Torr, 298 K, $[CH_3O_2]_0 = 3.8 \times 10^{11}$ molecule cm^{-3} and $[HO_2]_0 = 1.0 \times 10^{12}$ molecule cm^{-3} (■: actual data; ———: model).

CH_3O_2 decay are well predicted by the same model. However, as we pointed out in the previous paragraph, experimental conditions constrain our measurements to conditions of relatively slow rates of reactant decay (the decay presented in Figure 3 represents only about a 12% loss of CH_3O_2 over the reaction time accessed). Therefore, from this kinetics analysis standpoint, this first use of a fast-flow method for the CH_3O_2 + HO_2 reaction is at a disadvantage compared to earlier flash-photolysis studies in which larger peroxy radical decays were observed. We estimate that our measured decays are consistent with values between a factor of 0.7 (lower bound) and 1.3 (upper bound) of the JPL recommended value (which currently indicates an estimated upper-bound uncertainty factor of 2.0 at 298 K for this reaction [14]). However, if the uncertainties in the absolute concentrations of HO_2 and CH_3O_2 (as well as other potential systematic uncertainties) are considered, we estimate an overall upper-bound uncertainty factor for the overall rate constant of 1.7, which is a slight improvement over the current uncertainty value. However, it is important to point out that our detection methodology is more reliable than previous studies, in that our CIMS detection and calibration methods for CH_3O_2 and HO_2 are completely independent of one another (in contrast to the difficult UV detection problems presented by the overlapping peroxy radical spectra in those same flash-photolysis studies). Therefore, our TF-CIMS measurements of CH_3O_2 decay can be considered as complementary to the earlier flash-photolysis experiments in that, despite the fact that our fast-flow approach suffers by comparison in terms of extent of reaction observed, our chemical ionization detection technique is not hindered by the same detection complexities that plague UV detection of peroxy species.

Branching Channel Rate-Constant Determination

Figure 4 contains a kinetics plot ($[CH_3OOH]_{approx}$ vs. time) for an experiment performed at 100 Torr and 298 K (squares), as well as the predicted CH_3OOH rise (solid line) from a model calculation using the

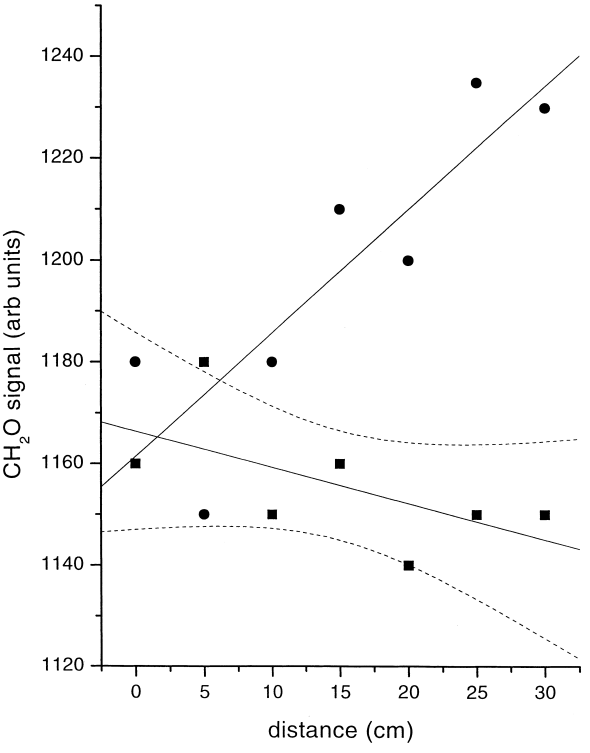

Figure 5 Observed production of CH_2O (●) from the CH_3O_2 + HO_2 reaction at 100 Torr, 298 K, $[CH_3O_2]_0 = 6.3 \times 10^{11}$ molecule cm^{-3} and $[HO_2]_0 = 1.0 \times 10^{12}$ molecule cm^{-3} as compared to the background signal (■) obtained with the HO_2 source turned off. Linear least squares fits to both data sets are plotted as solid lines to guide the eye, and the 95% confidence interval for the background data is plotted as dashed lines.

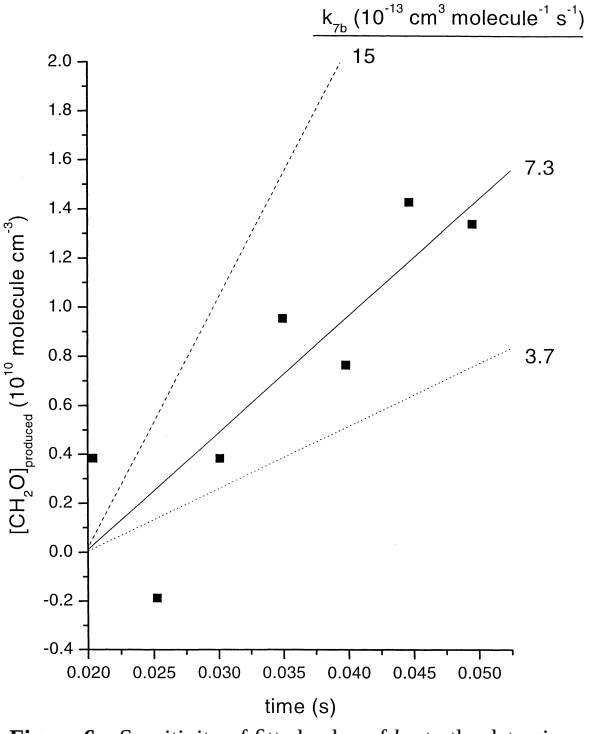

Figure 6 Sensitivity of fitted value of k_{7b} to the data given in Figure 5.

calibrated initial concentrations of CH_3O_2 and HO_2 and the reactions listed in Table I. Although the agreement between the experimental data and the model curve appears excellent, the lack of a formal calibration for CH_3OOH precludes the quantitative determination of the rate constant for this branching channel (k_{7a}). However, Figure 4 does provide confirming evidence that the CH_3OOH-producing branching channel is in fact the major product pathway for the $CH_3O_2 + HO_2$ reaction. We chose not to pursue the quantitative determination of k_{7a} because the partitioning between two competing channels is best determined by measurements of the minor channel (k_{7b}, in the case of $CH_3O_2 + HO_2$), which is described in the following paragraph.

The major complication in the rate-constant determination for the CH_2O producing channel (k_{7b}) is the CH_2O-producing side reaction resulting from the self-reaction of CH_3O_2:

$$CH_3O_2 + CH_3O_2 \longrightarrow CH_3O + CH_3O + O_2 \quad (21a)$$

$$\longrightarrow CH_2O + CH_3OH + O_2 \quad (21b)$$

$$\longrightarrow CH_3OOCH_3 + O_2 \quad (21c)$$

($k_{21} = 4.7 \times 10^{-13}$ cm^3 molecule^{-1} s^{-1}) [14]. Note that CH_2O is directly produced via reaction (21b) and indirectly produced via reaction (21a) in the presence of oxygen by coupling to reaction (11).

$$CH_3O + O_2 \longrightarrow CH_2O + HO_2 \quad (11)$$

At 298 K, the JPL recommendation for reaction (21) indicates the following branching ratios for channels a, b, and c, respectively: 0.3, 0.6, and 0.1 [14]. Therefore, 60% of the total $CH_3O_2 + CH_3O_2$ reactive events lead to CH_2O; in the presence of sufficient O_2, the fraction increases to 90% (also note that channel 21a produces two CH_2O molecules per reactive event, while channel 21b produces only one). For our experimental conditions ([O_2] $\sim 3.0 \times 10^{16}$ molecule cm^{-3}), the CH_2O-producing fraction is predicted to be near the limiting 90% value. Because main flow concentrations of CH_3O_2 are low ($<1.0 \times 10^{12}$ molecule cm^{-3}) compared to the overall rate constant, it might be expected that reaction (21) would lead to small CH_2O background levels. However, CH_3O_2 concentrations are about 15 times higher in the sidearm of the flow tube where it is produced, thus increasing the rate of the self-reactions given above before they enter the main flow tube. In fact, the sidearm reaction time was optimized (by varying the position in the sidearm where the F atoms were injected) to achieve the most favorable conditions (i.e., the largest CH_3O_2/CH_2O ratio possible). Using the relevant concentrations and times for CH_3O_2 self-reaction in the sidearm and a kinetic model incorporating the reactions given above, we estimate that for the largest main flow-tube concentrations of $[CH_3O_2]_0$ used (1.0×10^{12} molecule cm^{-3}), a "background" main flow-tube concentration of [CH_2O] $\sim 1.5 \times 10^{11}$ molecule cm^{-3} should be observed. This background source of CH_2O is a constant with respect to the kinetics data collected (the CH_3O_2 source is spatially fixed, and thus all reactions involving species originating from it have the same total reaction time regardless of the HO_2 injector position). Since none of the CH_2O-producing reactions listed in Table I depends on the presence of HO_2, we expect that any CH_2O produced from side reactions should not depend on the HO_2 injector position. However, it is possible that the additional O_2 added to the flow system through the HO_2 injector could lead to additional production of CH_2O via reactions (21a) and (11) that would appear to depend on the position of the HO_2 injector. In Figure 5, the raw CH_2O signal vs. injector distance data is presented for two experiments: The data depicted as circle symbols was collected with the HO_2 source on, and the data depicted as square symbols was collected with the HO_2 source off (all gases flowing, but the microwave discharge

was turned off). It is apparent from these experiments that no additional CH_2O is formed by the introduction of gases used to synthesize HO_2 (helium, hydrogen, and oxygen). It is also apparent that the CH_2O produced with the HO_2 source operating is statistically significant, as the CH_2O signal is observed rising above the 95% confidence interval for the CH_2O time-dependent profile obtained with the HO_2 source turned off. Using the CH_2O calibration factor and the total CH_2O signal observed for the experiments depicted in Figure 5, a background CH_2O level of about 1.7×10^{11} molecule cm^{-3} is calculated. As discussed above, this background level is consistent with kinetic model results for the production of CH_2O via CH_3O_2 self-reaction chemistry. In summary, despite the fact that a relatively large CH_2O background signal is observed (which is consistent with kinetic modeling of the CH_3O_2 self-reaction chemistry occurring in the side-arm reactor), we are able to observe CH_2O production as a function of HO_2 contact time that can be positively attributed to the CH_3O_2 + HO_2 reaction.

Figure 6 shows the CH_2O production observed (squares) for the reaction conditions given in Figure 5, with a solid line fit through the data to determine the rate of CH_2O production, which is used in the fitting process to determine k_{7b}. The value of k_{7b} was fitted by using a kinetic model that included the reactions and rate parameters given in Table I and the experimental initial concentrations of CH_3O_2, HO_2, and O_2 to calculate the rate of CH_2O production for comparison to the experimentally determined rate of CH_2O production. The value of k_{7a} in the fitting process was constrained by the relationship $k_{7a} = k_7 - k_{7b}$, where k_7 was calculated from the JPL-recommended Arrhenius parameters [14]. In Figure 6, along with fitted value for k_{7b} (solid line), k_{7b} values that are a factor of 2 higher (dashed line) and a factor of 2 lower (dotted line) are used to predict CH_2O profiles to illustrate the sensitivity of the fitted value of k_{7b} to the actual CH_2O profile observed. It is apparent from this plot and the statistical uncertainties reported in Table II that the fitted k_{7b} values are determined to a precision of about 50%.

The experiments were carried out at several different $[CH_3O_2]_0$ and $[HO_2]_0$ concentrations, which provide a test of consistency for the kinetic model and the method of data analysis. Table II lists the experimental conditions and fitted k_{7b} values (and associated branching ratios) for all experiments performed. In particular, several different $[CH_3O_2]_0$ values (at nearly fixed HO_2 concentrations) were used to test the consistency of the k_{7b} determination method. Figure 7 shows that very similar k_{7b} values were obtained for these experiments with differing initial CH_3O_2 concentrations. Although this test does not rule out other systematic errors in the fitting of k_{7b} (such as HO_2 calibration errors or

Table II Branching Ratio Data for the CH_3O_2 + HO_2 → CH_2O + H_2O + O_2 Reaction at 100 Torr Pressure

T (K)	$[CH_3O_2]_0$ (10^{10} molecule cm^{-3})	$[HO_2]_0$ (10^{10} molecule cm^{-3})	k_{7b} (and 1σ error) (10^{-14} cm^3 $molecule^{-1}$ s^{-1})	Branching Ratio $k_{7b}/(k_{7a} + k_{7b})$
298	39	125	56 ± 22	0.10
298	38	100	56 ± 39	0.10
298	92	100	45 ± 39	0.08
298	63	100	73 ± 28	0.13
298	42	115	67 ± 34	0.12
273	80	100	57 ± 50	0.08
273	88	100	71 ± 71	0.10
263	80	76	104 ± 40	0.13
263	80	76	104 ± 32	0.13
253	77	139	180 ± 54	0.20
253	77	139	144 ± 63	0.16
253	77	139	144 ± 63	0.16
253	77	139	135 ± 36	0.15
243	82	140	150 ± 40	0.15
243	82	140	150 ± 30	0.15
243	82	140	120 ± 50	0.12
237	60	139	231 ± 55	0.21
230	48	79	431 ± 130	0.35
230	50	79	357 ± 86	0.29
218	52	79	492 ± 130	0.33
218	52	79	447 ± 270	0.30

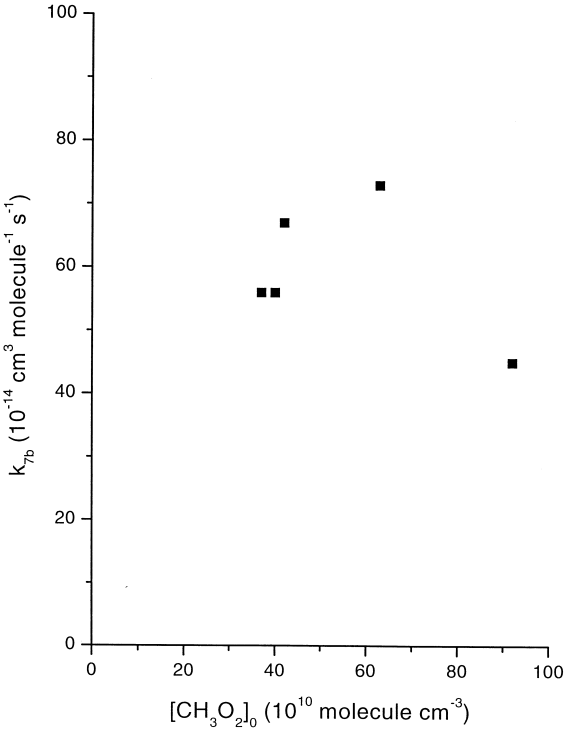

Figure 7 Dependence of the fitted $CH_3O_2 + HO_2 \rightarrow CH_2O + H_2O + O_2$ branching channel rate constant on initial CH_3O_2 concentration.

unknown sources of CH_2O originating from species produced in the HO_2 injector), it does suggest that the CH_3O_2 calibration is not subject to large systematic error, and thus the fitted values of k_{7b} are fairly reliable from the point of view of the modeled CH_3O_2 chemistry. The error given in Table II represents the statistical uncertainty determined in the fitting process and does not include contributions from systematic error. We have previously estimated that the largest source of systematic error in these types of experiments results from the titration/calibration methods used for HO_2 and CH_3O_2 [4]. We estimate that this error is on the order of $\pm 15\%$ (1σ) for these species as well as for the CH_2O calibration method. In addition, uncertainties in the rate constants used in the fitting process can also introduce systematic error to the determination of k_{7b} (in particular, the uncertainty in k_7, which propagates nearly linearly into the value of k_{7b}). There is also some uncertainty in the determination of absolute reaction time from the flow velocity and distance from the injector tip to the mass spectrometer sampling aperture. However, this uncertainty is probably fairly low since the flow velocity depends directly on the accuracy of the mass flow meters (calibrated to at least 5% accuracy) and the distance is uncertain to less than 1 cm (the distance between the ionization region and the mass spectrometer aperture), or about 2% of the longest reaction time. Nonetheless, it is clear that relatively large systematic errors (as much as 50%, 1σ) are potentially present in our fitted values for k_{7b}.

Based on our five fitted k_{7b} values at 298 K and 100 Torr, we calculate a value (and 1σ statistical uncertainty) for the branching ratio $[k_{7b}/(k_{7a} + k_{7b})]$ of 0.11 ± 0.02. Table III lists the product monitored, experimental conditions, and inferred values for the branching ratio from the previous indirect (CH_2O is not directly detected) studies as well as the present direct (CH_2O is directly detected) one. The kinetics study of Moortgat et al. [9] involved the simultaneous monitoring of peroxy radicals and CH_3OOH at 298 K and 700 torr, which allowed the determination of an overall rate constant (4.8×10^{-12} cm^3 molecule^{-1} s^{-1}; compared to the current JPL recommended value of 5.6×10^{-12} cm^3 molecule^{-1} s^{-1} used in this work) as well as a specific CH_3OOH-producing rate constant (3.5×10^{-12} cm^3 molecule^{-1} s^{-1}). From these rate constants, a CH_2O-producing branching ratio of 0.27 may be inferred. In the work of Jenkin et al. [8], CD_3O_2 was used as a reactant and the production of HDO was followed at 298 K and 11 torr. The branching ratio determined by Jenkin et al. was determined in a manner similar to the present work; the rate constant for HDO (formed along with CD_2O and O_2) pro-

Table III Comparison of Branching Ratio Determinations for the $CH_3O_2 + HO_2$ Reaction

Study	Product Monitored	Temperature (K)	Pressure (Torr)	$k_{7b}/(k_{7a} + k_{7b})$
Moortgat *et al.* [9]	CH_3OOH	298	700	0.27
Jenkin *et al.* [8]	HDO[a]	298	11	0.40
Wallington [16]	CH_3OOH	298	15–700	0.08 ± 0.05
This work	CH_2O	298	100	0.11 ± 0.02
This work	CH_2O	218–298	100	$\left[1 + e^{\left(\frac{-1160}{T} + 6.21\right)}\right]^{-1}$

[a] From measurements of the reaction $CD_3O_2 + HO_2 \rightarrow CD_2O + HDO + O_2$.

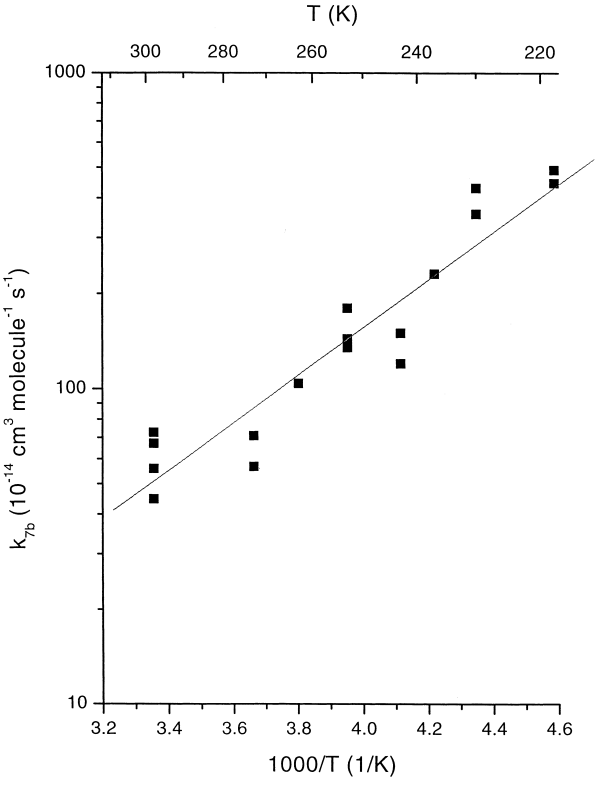

Figure 8 Arrhenius plot of the temperature dependence of the rate constant at 100 Torr pressure of the CH_3O_2 + $HO_2 \rightarrow CH_2O + H_2O + O_2$ branching channel (■: actual data; ———: fit to data).

duction was directly determined, and the branching ratio was determined by dividing this value by their value for the overall rate constant (5.4×10^{-12} cm^3 $molecule^{-1}$ s^{-1}). As Jenkin et al. point out, their CD_2O-producing branching ratio result of 0.40 for CD_3O_2 must be interpreted with care, as kinetic isotope effects are likely to make the CH_2O-producing results for CH_3O_2 somewhat different. Wallington [16] determined the fraction of CH_3OOH produced from the CH_3O_2 + HO_2 reaction at 298 K and several pressures by performing a carbon mass balance analysis. From the "missing carbon," a CH_2O-producing branching ratio of 0.08 may be inferred. Our direct result is in excellent agreement with the inferred result of Wallington [16], while it is substantially lower than the values inferred from the work of Moortgat et al. [9] and Jenkin et al. [8].

Temperature Dependence of the CH_2O Branching Channel Rate-Constant Determination

In order to establish a set of branching ratio values for the whole range of tropospherically relevant temperatures, we performed several measurements of k_{7b} at temperatures between 218 and 298 K in order to determine the temperature dependence of the CH_2O branching channel. From the data listed in Table II and plotted in Figure 8, we obtained the following Arrhenius expression (with 1σ statistical uncertainties): $k_{7b}(T) = 1.6^{+1.0}_{-0.7} \times 10^{-15} \times \exp[(1730 \pm 130)/T]$ cm^3 $molecule^{-1}$ s^{-1}. It is clear from the data and the fitted Arrhenius expression that both k_{7b} and the branching ratio (k_{7b} increases even more quickly than k_7 as the temperature decreases) show a steep negative temperature dependence: k_7 increases by a factor of ~7, and the branching ratio increases by a factor of ~3 as the temperature is decreased from 298 to 218 K. The negative temperature dependence of k_7 is consistent with the formation of a reactive intermediate. Figure 9 depicts a potential mechanism for reaction (7b) that is based on a six-membered ring intermediate structure that rearranges to produce the observed products. The more dramatic negative temperature dependence of k_{7b} suggests that the CH_2O-producing product channel is even more dependent on efficient thermal stabilization of the intermediate than is the CH_3OOH-producing channel. Given the very specific intermediate geometry required for the CH_2O-forming mechanism shown in Figure 9, the steep negative temperature dependence of k_{7b} seems consistent with the proposed mechanism.

Since the CH_3O_2 + CH_3O_2 reaction has similar product channels to the CH_3O_2 + HO_2 reaction, it is of interest to compare the temperature dependences of the branching ratios for these reactions. There have been several previous studies of the temperature dependence of the branching channels for the CH_3O_2 + CH_3O_2 reaction (for a review, see ref. [25]). Although other workers have reported the existence of a CH_3OOCH_3-producing channel (reaction (21c)), the most recent work of Tyndall et al. indicates no evidence for that channel (an upper limit of 6% is estimated) [26]. Accordingly, one can consider the temperature dependence of just the two major product channels for the CH_3O_2 + CH_3O_2 reaction:

$$CH_3O_2 + CH_3O_2 \longrightarrow CH_3O + CH_3O + O_2 \quad (21a)$$

$$\longrightarrow CH_2O + CH_3OH + O_2 \quad (21b)$$

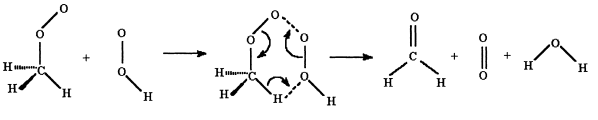

Figure 9 Proposed mechanism for the CH_3O_2 + $HO_2 \rightarrow$ $CH_2O + H_2O + O_2$ branching channel.

In these experiments, a branching ratio, defined as $\alpha = [k_{21a}/(k_{21a} + k_{21b})]$, was measured as a function of temperature. In order to allow an Arrhenius analysis, the branching ratio data were converted to the ratio defined as $\beta = k_{21a}/k_{21b}$. In order to generalize this ratio to the $CH_3O_2 + HO_2$ analysis as well, this term can be thought of as the ratio of the "direct" O_2 elimination channel to the "indirect" (hydrogen transfer) O_2 elimination channel. For both $CH_3O_2 + CH_3O_2$ and $CH_3O_2 + HO_2$, the "indirect" channel produces CH_2O. Based on all available data, Lightfoot et al. obtained the following Arrhenius-type expression for $CH_3O_2 + CH_3O_2$: $\ln \beta = 3.22 - 1165/T$ [25]. In order to directly compare the temperature dependence of the branching ratio obtained for the $CH_3O_2 + HO_2$ reaction with that for $CH_3O_2 + CH_3O_2$, we also recast our data in terms of β ($= k_{7a}/k_{7b}$ for $CH_3O_2 + HO_2$) and obtained the following Arrhenius-type expression: $\ln \beta = 6.21 - 1160/T$. These expressions reveal remarkable agreement in the temperature dependence of the CH_2O producing channels for the $CH_3O_2 + CH_3O_2$ and $CH_3O_2 + HO_2$ reactions. The $C_2H_5O_2 + C_2H_5O_2$ reaction proceeds through analogous product channels to produce CH_3CHO, albeit at smaller branching ratio at 298 K (0.3 for the direct CH_3CHO-producing channel) as well as a less steep negative temperature dependence ($\ln \beta = 2.32 - 533/T$) than for $CH_3O_2 + CH_3O_2$ [25]. Current experimental evidence obtained at 298 K seems to indicate that the $C_2H_5O_2 + HO_2$ reaction does not have a significant CH_3CHO-producing channel [27]. However, our finding that the CH_2O-producing channels for $CH_3O_2 + CH_3O_2$ and $CH_3O_2 + HO_2$ have similarly strong negative temperature dependences may indicate that the $C_2H_5O_2 + HO_2$ reaction has the potential to have a significant CH_3CHO-producing channel at low temperatures. Finally, from our definition of $\beta = k_{7a}/k_{7b}$, we can derive a convenient term for the temperature dependence of the CH_2O branching ratio for the $CH_3O_2 + HO_2$ reaction:

$$k_{7b}/(k_{7a} + k_{7b}) = 1/(1 + \beta) = [1 + e^{(-1160/T + 6.21)}]^{-1} \quad (22)$$

Atmospheric Significance of CH_2O Production from $CH_3O_2 + HO_2$ Reaction

As we have established that the $CH_3O_2 + HO_2$ reaction possesses a significant CH_2O-producing branching channel (which increases in significance as the temperature is lowered), it is of interest to consider how this result may impact atmospheric models, which generally assume a branching ratio of zero for the CH_2O-producing channel. Because high NO_x levels circumvent CH_2O production via either $CH_3O_2 + HO_2$ pathway [reactions (4a) and (11) instead determine the rates of CH_2O production], we expect that reaction (7b) is of minor significance in highly polluted environments. However, we propose two potential impacts on the prediction accuracy of atmospheric models in environments (relatively low NO_x) where significant direct CH_2O production via reaction (7b) can occur. The atmospheric fate of CH_3OOH (the main channel product of the $CH_3O_2 + HO_2$ reaction) is also the eventual formation of CH_2O:

$$CH_3OOH + h\nu \longrightarrow CH_3O + OH \quad (23)$$

$$CH_3O + O_2 \longrightarrow CH_2O + HO_2 \quad (11)$$

An obvious potential effect is that if the reaction (7b) pathway is faster than the reaction (7a/23/11) pathway currently used in atmospheric models, one would expect that observed CH_2O levels might be higher than predicted. From the atmospheric lifetimes for the relevant species (derived using background NO_x levels) presented in Lawrence et al., it does appear that the reaction (7b) pathway (~hours) should be significantly faster than the reaction (7a/23/11) pathway (~days), which is limited by the relatively long lifetime of CH_3OOH against photolysis [28]. In fact, Ayers et al. had earlier found that observed CH_2O levels at Cape Grim, Tasmania (a location characterized by very low NO_x levels), were underpredicted by atmospheric models, which assumed a k_{7b} value of zero [17]. However, Ayers et al. found that a branching ratio of 0.40 was required to reconcile the observed CH_2O levels with the model results, a value significantly larger than the one reported here. More recently, Weller et al. reported the results of CH_2O measurements in the marine boundary layer of the Atlantic and came to a similar conclusion: Observed CH_2O levels were greater than the predictions from a photochemical model using a k_{7b} value of zero [18]. Following the earlier work of Ayers et al., Weller et al. added reaction (7b) to their model (again with a branching ratio of 0.40) and found that the predicted CH_2O concentrations were in closer (although not full) agreement with their atmospheric observations. Therefore, although our present study presents evidence for a significant CH_2O-forming product channel from the $CH_3O_2 + HO_2$ reaction, it appears that the k_{7b} value determined here will not fully reconcile model predictions and atmospheric observations of CH_2O.

A less obvious effect of nonnegligible CH_2O production via reaction (7b) might involve a modification of the efficiency of HO_x cycling. CH_2O itself has only

a short atmospheric lifetime against photolysis (~hours) [28]:

$$CH_2O + h\nu \longrightarrow H_2 + CO \quad (24a)$$

$$\longrightarrow H + HCO \quad (24b)$$

with the two branching channels being roughly equal for overhead solar conditions [29]. Both products of reaction (24b) lead to the formation of HO_2:

$$H + O_2 + M \longrightarrow HO_2 + M \quad (14)$$

$$HCO + O_2 \longrightarrow HO_2 + CO \quad (25)$$

Therefore, the existence of a significant CH_2O-producing channel for the CH_3O_2 + HO_2 reaction could lead to faster HO_x regeneration simply because CH_2O is produced faster via reaction (7b) than via reactions (7a/23/11). This effect may be a contributing factor in the search for an answer to the observation that observed HO_x levels in the upper troposphere are greater than those predicted by current atmospheric models (which assume a value of zero for k_{7b}) [5].

CONCLUSIONS

The results presented here represent the first direct measurement of the CH_2O-producing channel of the CH_3O_2 + HO_2 reaction, as well as the first product-specific temperature-dependence study of any kind for this reaction. The kinetics of the reactant CH_3O_2 and the main branching channel product CH_3OOH were also monitored and found to be consistent with JPL recommendation for the overall rate constant [14]. This study indicates the CH_3O_2 + HO_2 reaction should be a significant source of CH_2O in the troposphere, as the branching ratio $[k_{7b}/(k_{7a} + k_{7b})]$ at 100 Torr was found to be 0.11 at 298 K and increased to 0.31 as the temperature was lowered to 218 K. This work should help improve the kinetics database for methane oxidation chemistry by placing more stringent constraints on CH_2O and HO_x formation and destruction rates. In particular, these findings may help explain larger-than-predicted (by models which assume a k_{7b} value of zero) CH_2O observations in the clean troposphere, as well as larger-than-predicted HO_x levels in the upper troposphere.

This research was funded by grants from the National Science Foundation (ATM-9874752), the Towsley Foundation, the Camille and Henry Dreyfus Foundation, the American Chemical Society–Petroleum Research Fund, and Research Corporation.

BIBLIOGRAPHY

1. Finlayson-Pitts, B. J.; Pitts, J. N. Chemistry of the Upper and Lower Atmosphere; Academic Press: San Diego, 1999.
2. Bertman, S. B.; Roberts, J. M.; Parrish, D. D.; Buhr, M. P.; Goldan, P. D.; Kuster, W. C.; Fehsenfeld, F. C.; Montzka, S. A.; Westberg, H. J Geophys Res 1995, 100, 22805.
3. Flocke, F.; Atlas, E.; Madronich, S.; Schauffler, S. M.; Aikin, K.; Margitan, J. J.; Bui, T. P. Geophys Res Lett 1998, 25, 1891.
4. Scholtens, K. W.; Messer, B. M.; Cappa, C. D.; Elrod, M. J. J Phys Chem A 1999, 103, 4378.
5. Wennberg, P. O.; Hanisco, T. F.; Jaeglé, L.; Jacob, D. J.; Hintsa, E. J.; Lanzendorf, E. J.; Anderson, J. G.; Gao, R.; Keim, E. R.; Donnelly, S. G.; Negro, L. A.; Fahey, D. W.; McKeen, S. A.; Salawitch, R. J.; Webster, C. R.; May, R. D.; Herman, R. L.; Proffitt, M. H.; Margitan, J. J.; Atlas, E. L.; Schauffler, S. M.; Flocke, F.; McElroy, C. T.; Bui, T. P. Science 1998, 279, 49.
6. Cox, R. A.; Tyndall, G. S. Chem Phys Lett 1979, 65, 357.
7. Cox, R. A.; Tyndall, G. S. J Chem Soc, Faraday Trans 2 1980, 76, 153.
8. Jenkin, M. E.; Cox, R. A.; Hayman, G. D.; Whyte, L. J. J Chem Soc, Faraday Trans 2 1988, 84, 913.
9. Moortgat, G. K.; Cox, R. A.; Schuster, G.; Burrows, J. P.; Tyndall, G. S. J Chem Soc, Faraday Trans 2 1989, 85, 809.
10. McAdam, K.; Veyret, B.; Lesclaux, R. Chem Phys Lett 1987, 133, 39.
11. Kurylo, M. J.; Dagaut, P.; Wallington, T. J.; Neuman, D. M. Chem Phys Lett 1987, 139, 513.
12. Dagaut, P.; Wallington, T. J.; Kurylo, M. J. J Phys Chem 1988, 92, 3833.
13. Lightfoot, P. D.; Veyret, B.; Lesclaux, R. J Phys Chem 1990, 94, 708.
14. DeMore, W. B.; Sander, S. P.; Howard, C. J.; Ravishankara, A. R.; Golden, D. M.; Kolb, C. E.; Hampson, R. F.; Kurylo, M. J.; Molina, M. J. Chemical Kinetics and Photochemical Data for Use in Stratospheric Modeling JPL Publication 97-4, Jet Propulsion Laboratory: Pasadena, California, 1997.
15. Kan, C. S.; Calvert, J. G.; Shaw, J. H. J Phys Chem 1980, 84, 3411.
16. Wallington, T. J. J Chem Soc, Faraday Trans 1991, 87, 2379.
17. Ayers, G. P.; Gillett, R. W.; Granek, H.; de Serves, C.; Cox, R. A. Geophys Res Lett 1997, 24, 401.
18. Weller, R.; Schrems, O.; Boddenberg, A.; Gab, S.; Gautrois, M. J Geophys Res 2000, 105, 14401.

19. Seeley, J. V.; Jayne, J. T.; Molina, M. J. Int J Chem Kinet 1993, 25, 571.
20. Ranschaert, D. L.; Schneider, N. J.; Elrod, M. J. J Phys Chem A 2000, 104, 4449.
21. Elrod, M. J.; Meads, R. F.; Lipson, J. B.; Seeley, J. V.; Molina, M. J. J Phys Chem 1996, 100, 5808.
22. Midey, A. J.; Arnold, S. T.; Viggiano, A. A. J Phys Chem A 2000, 104, 2706.
23. Huey, L. G.; Hanson, D. R.; Howard, C. J. J Phys Chem 1995, 99, 5001.
24. Messer, B. M.; Stielstra, D. E.; Cappa, C. D.; Scholtens, K. W.; Elrod, M. J. Int J Mass Spectrom 2000, 197, 219.
25. Lightfoot, P. D.; Cox, R. D.; Crowley, J. N.; Destriau, G. D.; Hayman, G. D.; Jenkin, M. E.; Moortgat, G. K.; Zabel, T. Atmos Env 1992, 26A, 1805.
26. Tyndall, G. S.; Wallington, T. J.; Ball, J. C. J Phys Chem A 1998, 102, 2547.
27. Wallington, T. J.; Japar, S. M. Chem Phys Lett 1990, 166, 495.
28. Lawrence, M. G.; Crutzen, P. J.; Rasch, P. J.; Eaton, B. E.; Mahowald, N. M. J Geophys Res Atmos 1999, 104, 26245.
29. Seinfeld, J. H.; Pandis, S. N. Atmospheric Chemistry and Physics; John Wiley and Sons, Inc.: New York, 1998.